International Journal of Nanomedicine

Dovepress
open access to scientific and medical research

Open Access Full Text Article

ORIGINAL RESEARCH

Preparation, Optimization, and Anti-Pulmonary Infection Activity of Casein-Based Chrysin Nanoparticles

Huaqiao Tang[1,*], Liying Dong[1,*], Xue Xia[1,*], Xinling Chen[1], Meichen Ren[1], Gang Shu[1], Hualin Fu[1], Juchun Lin[1], Ling Zhao[1], Li Zhang[2], Guoqiang Cheng[2], Xianxiang Wang[3], Wei Zhang[1]

[1]College of Veterinary, Sichuan Agricultural University, Chengdu, 611130, People's Republic of China; [2]Sichuan Academy of Chinese Medicine Sciences, Chengdu, 610041, People's Republic of China; [3]College of Science, Sichuan Agricultural University, Chengdu, 611130, People's Republic of China

*These authors contributed equally to this work

Correspondence: Wei Zhang, Email Zhangwei26510c@126.com

Introduction: Chrysin has a wide range of biological activities, but its poor bioavailability greatly limits its use. Here, we attempted to prepare casein (cas)-based nanoparticles to promote the biotransfer of chrysin, which demonstrated better bioavailability and anti-infection activity compared to free chrysin.

Methods: Cas-based chrysin nanoparticles were prepared and characterized, and most of the preparation process was optimized. Then, the in vitro and in vivo release characteristics were studied, and anti-pulmonary infection activity was evaluated.

Results: The constructed chrysin-cas nanoparticles exhibited nearly spherical morphology with particle size and ζ potential of 225.3 nm and −33 mV, respectively. These nanoparticles showed high encapsulation efficiency and drug-loading capacity of 79.84% ± 1.81% and 11.56% ± 0.28%, respectively. In vitro release studies highlighted a significant improvement in the release profile of the chrysin-cas nanoparticles (CCPs). In vivo experiments revealed that the relative oral bioavailability of CCPs was approximately 2.01 times higher than that of the free chrysin suspension. Further investigations indicated that CCPs effectively attenuated pulmonary infections caused by *Acinetobacter baumannii* by mitigating oxidative stress and reducing pro-inflammatory cytokines levels, and the efficacy was better than that of the free chrysin suspension.

Conclusion: The findings underscore the advantageous bioavailability of CCPs and their protective effects against pulmonary infections. Such advancements position CCPs as a promising pharmaceutical agent and candidate for future therapeutic drug innovations.

Keywords: chrysin, nanoparticles, *Acinetobacter baumannii*, casein

Introduction

Chrysin, a flavonoid abundant in passion flowers, honey, and propolis, exhibits diverse pharmacological properties, which include anti-inflammatory, antioxidant, anti-allergic, anti-diabetic, and anti-tumor activities.[1] Chrysin exhibited robust anti-inflammatory properties in an investigation of smoke-induced acute respiratory inflammation in mice by inhibiting activation of the MAPK pathway and protecting against lung injury.[2] Chrysin mitigated lipopolysaccharide-induced acute lung injury in mice by improving vascular permeability and reducing pulmonary tissue inflammation.[3] Extensive research has identified chrysin as a promising therapeutic agent in diverse disease models, while its poor water solubility, low intestinal absorption, significant first-pass effect, diminished oral bioavailability, weak in vivo efficacy, and rapid systemic elimination greatly limit its wider application.[4]

Conventional formulations encounter difficulties in improving solubility associated with poorly soluble drugs. Nanoparticles have gained recognition as an innovative drug delivery system extensively utilized for administering drugs with poor water solubility. Casein, the principal protein in milk, demonstrates substantial stability, safety, non-toxicity, inherent biocompatibility, and biodegradability. These attributes position it as an ideal drug delivery carrier for enhancing bioavailability.[5,6] Cas is a deblock copolymer with amphiphilic structures capable of self-assembling in water, forming core-shell complexes. The hydrophobic

Received: 2 January 2024
Accepted: 29 May 2024
Published: 10 June 2024

inner chains aggregate to form the core, while the hydrophilic outer chains create the shell of the complex.[7] This allows for the physical entrapment or chemical conjugation of hydrophobic drugs within the core, enabling the development of innovative nano-drug delivery systems.[8] Cas-based drug delivery systems improved the solubility and bioavailability of poorly soluble drugs to amplify drug dissolution and increased drug release rates by 1.5–2 times.[9,10] Cas was shown to protect oral and esophageal epithelium from drug-induced toxicity, establishing it as a promising candidate for oral drug delivery.[11] No documented studies have specifically centered on cas-loaded chrysin. Therefore, this study aimed to increase the bioavailability of chrysin by the combined application of cas and chrysin to augment its solubility.

Acinetobacter baumannii (Ab) is a widespread gram-negative coccobacillus bacterium lacking flagella, often identified as a dangerous pathogen in infections, leading to conditions like bacteremia, pneumonia, endocarditis, and skin infections. The pathogenesis of Ab primarily involves bacterial adhesion to host cells, the formation of bacterial biofilms, colonization, and the prolific production of capsular polysaccharides (CPSs). These CPSs encapsulate the outer membrane, forming a crucial mucoid layer that facilitates bacterial adhesion.[12] Numerous Ab strains demonstrate pronounced drug resistance, which limits alternative treatments to colistin and tigecycline, the sole effective medications for this infection.[13,14] Hence, the World Health Organization has classified Ab as a bacterium requiring urgent research and development of new antimicrobial drugs. Research suggests that chrysin can disrupt the outer membrane of Ab cells, modify their bacterial membrane potential, and inhibit biofilm formation.[15] However, challenges arise in conducting in vivo studies regarding the effects of chrysin on Ab due to its low oral bioavailability, weak efficacy, and rapid systemic elimination upon oral administration.

This study aimed to develop and optimize a preparation of CCPs while conducting comprehensive characterizations to assess the stability of the complex, thus highlighting cas's carrier properties encapsulating chrysin. Particle size, the polydispersity index (PDI) value, and ζ-potential of the synthesized particles were evaluated. Subsequently, the CCPs were characterized using differential scanning calorimetry (DSC), X-ray diffraction (XRD), transmission electron microscopy (TEM), and Fourier-transform infrared spectroscopy (FTIR). In vitro release studies and pharmacokinetic investigations were conducted to assess the potential of cas to enhance absorption and oral bioavailability. In vivo experiments were conducted to evaluate the protective effects of CCPs against Ab infection.

Materials and Methods

Materials

Chrysin was provided by Chengdu JM BioPharm Co., Ltd. (Chengdu, China), while cas was procured from Sigma-Aldrich (USA). Thermo Fisher Scientific supplied sodium dodecyl sulfate (SDS) for high-performance liquid chromatography (HPLC). Chromatographic-grade formic acid, acetonitrile, and methanol used in liquid chromatography were sourced from Tianjin Kermel Chemical Reagent Co., Ltd. (Tianjin, China). All other reagents used in the experiments were analytical grade.

Preparation and Optimization of CCPs

CCPs were prepared with minor adjustments made to a previously published method.[16] Initially, an appropriate quantity of chrysin was dissolved in an ethanol solution. A precisely formulated casein solution was agitated on a magnetic stirrer for a specific duration and speed. Subsequently, the chrysin ethanol solution was introduced into the fully expanded casein solution under ice bath conditions. Following ultrasonication with a fixed-power probe, the CCP nanocomposite material was obtained. Finally, CCPs underwent a 48-hour pre-freezing phase, followed by a 24-hour freeze-drying process in a lyophilizer (LyoQuest, Telstar, Spain) to yield lyophilized CCP powder.

An orthogonal design based on single-factor experiments was employed to optimize the preparation process. Initially, single-factor experiments were conducted while keeping other variables constant to examine the impact of the cas concentration, chrysin input amount, magnetic stirrer speed, and ultrasonication duration on encapsulation efficiency. Subsequently, 3–4 factors with significant influence were selected as independent variables. The synthesis factors were optimized using CCP encapsulation efficiency as the indicator.

Encapsulation Efficiency and CCP Drug Loading

Encapsulation efficiency and CCP drug loading were assessed using HPLC. Initially, 2.0 mL of CCP solution was centrifuged at 12,000 rpm for 10 minutes using a filtration device (MWCO 10 kDa, Millipore, USA) to isolate free CCPs. The resulting filtrate was diluted and subsequently analyzed by HPLC to quantify the content of unbound chrysin. Simultaneously, an equivalent volume of the CCP suspension was meticulously measured and subjected to ultrasonication, followed by HPLC analysis to determine the total chrysin content. The encapsulation efficiency (EE) and loading efficiency (LE) were calculated using the following formulas:[17]

$$EE\,(\%) = \frac{\text{actual amount of CHN loaded in CHN} - \text{Cas}}{\text{initial amount of CHN}}$$

$$LE\,(\%) = \frac{\text{weight of CHN loaded in CHN} - \text{Cas}}{\text{weigh of CHN} - \text{Cas}}$$

HPLC Analysis of Chrysin

Chromatographic Conditions

An Agilent C18 column (4.6 mm×250 mm, 5 μm) with a mobile phase of acetonitrile-0.15% formic acid (65:35); a wavelength of 266 nm; flow rate of 1.0 mL·min-1; column temperature of 30 °C; and sample volume of 20 uL were used.

Linear Relationship

The relationship between chrysin concentrations (C) and peak areas (A) was assessed using regression analysis, which indicated linearity at Y=58.31x-106.31 (R2=0.999) Recovery and precision.

Low, medium, and high concentrations of a chrysin reference substance were added to a blank nanoparticle solution to calculate the sample recovery rate. The recovery of chrysin ranged from 95.36% to 98.85%. The findings indicated that the ultrafiltration membrane did not retain chrysin and had minimal impact on the experimental outcomes. The peak RSD area of the chrysin reference solution was continuously measured six times on the same day. Each measurement showed less than 2% variation.

Characterization of the Nanoparticles' Physicochemical Properties

The particle size, PDI, and ζ-potential of CCPs were determined using a Zetasizer Nano-ZS (Malvern, UK). CCP morphology was assessed by TEM imaging (HT7700, Hitachi, Japan). DSC thermograms were generated using an 1100 LF DSC instrument (Mettler Toledo, China). XRD analysis (D8 ADVANCE, Bruker, Germany) was performed on chrysin, cas, their physical blends, and CCPs to study their diffraction patterns. The FTIR spectra of chrysin, cas, and the CCP formulations were acquired by grinding samples with potassium bromide and scanning from 4000 to 400 cm using a Fourier-transform infrared spectrometer (Spectrum Two, PerkinElmer, USA).

In vitro Release Study

The in vitro drug release study utilized the dialysis bag method with 900 mL of a 0.5% SDS solution as the dissolution medium. A 3.0 mL volume of CCPs was enclosed in a dialysis bag with a 10 kDa molecular weight cutoff and submerged in a consistent-temperature water bath shaker set at 37 °C and 75 rpm. A similar procedure was performed for the chrysin suspension. Sampling occurred at 0, 30 minutes, 1, 2, 4, 8, 12, 24, and 49-hour intervals, where 3 mL of the dissolution medium was withdrawn and replaced to maintain consistent volume and absorption conditions. HPLC analysis was conducted on the withdrawn medium to generate release profiles.

Pharmacokinetic Study

All experimental procedures involving animals were conducted following the guidelines set by the Animal Welfare and Ethics Committee of Sichuan Agricultural University (Approval No. 20230045). Sprague-Dawley male rats (265 ± 15 g) were sourced from SPF Biotechnology Co., Ltd. (Beijing, China). All animals were housed in a controlled environment maintained at 24 ± 1°C with a 12-hour light-dark cycle. The rats were segregated into two groups (n = 6), with an equal distribution of

males and females, provided with free access to water, and underwent a 12-hour fasting period. Oral doses of 10 mg/kg of CCP solution or chrysin suspension and 20 mg/kg of chrysin suspension were administered via gavage. Blood samples of 0.5 mL were obtained from the orbital venous plexus into heparinized tubes at specified time intervals (0.083, 0.25, 0.5, 1, 2, 4, 6, 8, and 12 hours). The serum was isolated, underwent methanol precipitation, and was subsequently subjected to HPLC analysis to compare the pharmacokinetic parameters between the two groups using the method described in HPLC Analysis of Chrysin.

Anti-Pneumonia Study

Experimental Design

Male ICR mice (18–20 g, 6 weeks old) were acquired from SPF Biotechnology Co., Ltd. and were provided with unrestricted access to food and water. The mice were randomly divided into seven groups (n = 10): the blank control group (treated with saline), the model group (infected with Ab), the chrysin control group (Ab + 30 mg/kg chrysin), the cas control group (Ab + 30 mg/kg cas), and the CCP groups (Ab + 10, 20, and 30 mg/kg CCPs). Chrysin, cas, and CCPs were individually administered for three consecutive days. Following a 1-hour interval post-administration on the third day, the mice were intratracheally instilled with 30 μL of Ab (1×10^9 CFU/mL) to induce lung infections. Lung and blood samples were collected 24 hours after an infection was established.

Histopathological Analysis

In this study, the left lung tissues of mice were fixed in formalin and embedded in paraffin. Sections (5 μm) were cut and stained with hematoxylin and eosin (H&E) to visualize morphological changes following treatment with chrysin, cas, and CCP.s Optical microscopy (Olympus, Japan) was utilized to observe the stained sections and analyze pulmonary pathological alterations.

Analysis of Blood Cells

At the end of the mouse study, 0.5 mL of blood was collected from each mouse into EDTA anticoagulant tubes for blood counting analysis using an automated hematology analyzer. The analyzed parameters included white blood cell counts, lymphocyte percentage, monocyte percentage, neutrophil percentage.

Bacterial Load in the Tissues

Lung tissues were homogenized at a 1:9 ratio with sterile phosphate-buffered saline to assess bacterial colonization. Serial dilutions of homogenate were plated onto Luria-Bertani agar plates and incubated at 37 °C overnight. Subsequently, colonies were counted on plates with 30 to 300 colonies.

Measurement of Oxidative Stress

The levels of catalase (CAT), superoxide dismutase (SOD), malondialdehyde (MDA), and glutathione peroxidase (GSH-Px) were measured using commercially available assay kits from Jiancheng Bioengineering Institute (Nanjing, Jiangsu, China) according to the manufacturer's instructions to assess oxidative stress levels in the tissues.

Measurement of Inflammatory Cytokines

Levels of tumor necrosis factor (TNF)-α, interleukin (IL)-1β, and IL-6 cytokines in lung homogenates and serum samples were measured using enzyme-linked immunosorbent (ELISA) assay kits obtained from Jiangsu Meimian Industrial Co., Ltd.

Statistical Analysis

All in vitro assays were conducted in triplicate. The results are presented as means with standard deviations ($\overline{X} \pm SD$). Statistical analyses were conducted using one-way ANOVA followed by Tukey's post hoc test (IBM SPSS Statistics version 25, IBM, USA). Statistical significance was indicated at p-values of < 0.05 and < 0.01.

Results

Preparation of CCPs

The assessment of encapsulation efficiency and drug loading showed that the optimal process for preparing CCPs involved magnetic stirring at 500 rpm, incorporating 10 mg of chrysin with a cas concentration of 30 mg/mL (Figure 1). Orthogonal optimization was conducted under the described conditions to ascertain the best preparation procedure for CCPs, followed by

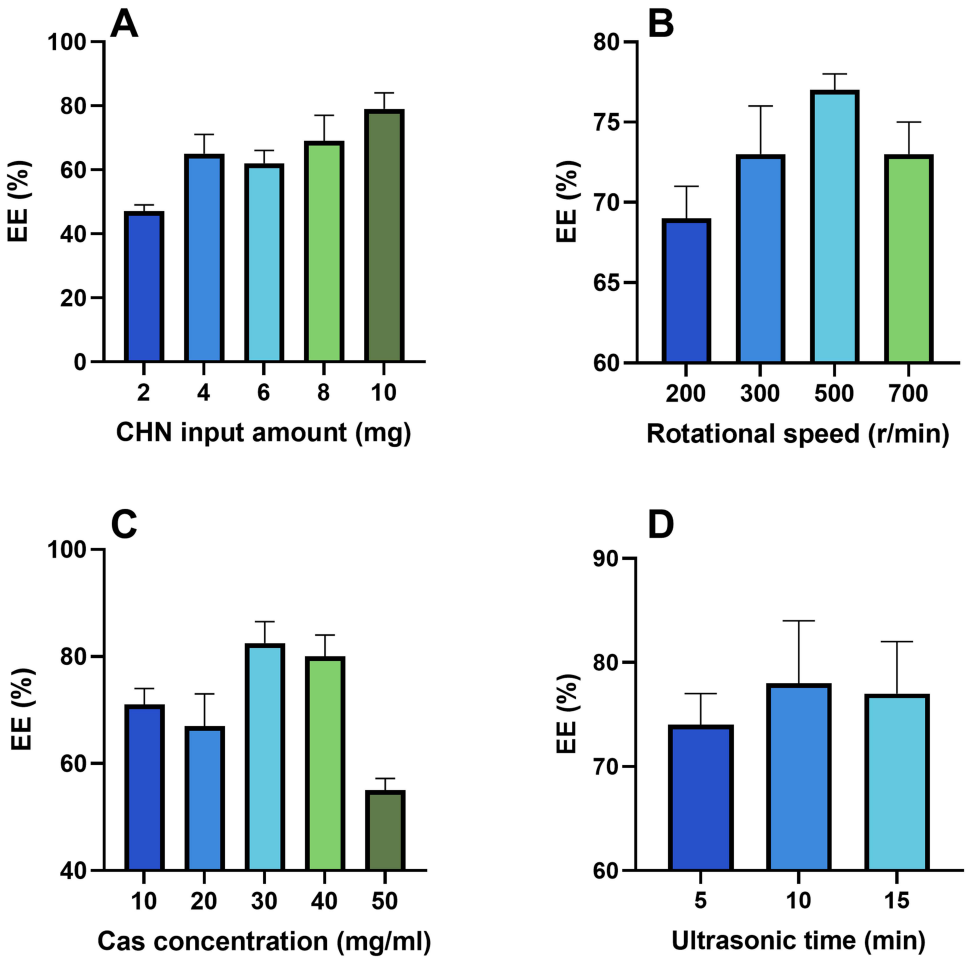

Figure 1 The influence of various factors on the encapsulation efficiency of CCPs (EE). Effect of chrysin input (**A**), magnetic stirring speed (**B**), cas concentration (**C**) and ultrasonic treatment time (**D**) on EE.

validation experiments (Table 1). Freeze-drying has been shown to preserve the stability of drugs in powdered form for at least six months and potentially longer, indicating its efficacy in maintaining long-term drug stability.[18] After preparing CCPs by the optimized formulation process, the encapsulation efficiency was 79.84% ± 1.81%, with a drug loading of 11.56% ± 0.28%. These values are comparable to those observed for benzylamine-casein nanocomposites.[19] Post-freeze-drying, there was a notable enhancement in encapsulation efficiency, indicating that it is an effective means for the long-term stable preservation of CCPs.

Physical and Chemical Characterization of CCPs

Particle Size, ζ-Potential, and Morphology

Particle size is a critical parameter for assessing nanoparticles, influencing their stability, drug release, biodistribution, and cellular uptake.[17] The CCP nanoparticles demonstrated a diameter of 225.3 nm with a PDI of 0.27, indicating a relatively homogeneous particle size distribution within a range from 0 to 0.3 (Figure 2A). The sizes was 31.03±5.59 nm in TEM (Supplementary Material, Table S1), which was difference with the results tested by Zetasizer. We speculate that the sample may be dropped on the grid to dry naturally when preparing TEM samples. In this process, the nanoparticles may aggregate and deform due to surface tension, solvent evaporation rate or temperature change, resulting in a decrease in particle size under electron microscopy. The 225.3 nm-sized CCP particles comprised hydrophobic regions that encapsulated chrysin within cas nanoaggregates, with diameters approximately ten times larger than those of blank cas nanoparticles.[6] The investigation by Sona et al focused on casein-based nanocomplexes designed to deliver amphotericin B, and revealed a reduction in particle size to 227 nm, consistent with the outcomes observed in this experiment.[20]

Table 1 Orthogonal Experimental Results

Item	Level	Chrysin Concentration	Cas Concentration	Ultrasonic Treatment Time
K-value	2	1.45	–	–
	6	1.93	–	–
	10	2.31	1.77	–
	30	–	2.00	–
	50	–	1.92	–
	300	–	–	1.89
	500	–	–	1.99
	700	–	–	1.81
K-means	2	0.48	–	–
	6	0.64	–	–
	10	0.77	0.59	–
	30	–	0.67	–
	50	–	0.64	–
	300	–	–	0.63
	500	–	–	0.66
	700	–	–	0.60
The best level		10	30	500
R		0.29	0.08	0.06
Level quantity		3	3	3
Number of repetitions per level		3.0	3.0	3.0

Zeta potential plays a pivotal role in maintaining nanoparticle stability. As the zeta potential increases, it enhances the repulsive forces among nanoparticles, effectively preventing their agglomeration.[21] The zeta potential typically needs to exceed ±30 mV.[22] The zeta potential value of CCP was −33 mV (Figure 2B), indicating a negatively charged surface. This negative charge generated repulsive forces,[23] promoting increased repulsion among the micelles, effectively inhibiting flocculation and aggregation and ensuring the stability of the CCP solution.[24]

The utilization of ultrasonic dispersion and shearing enhances the uniformity of particle size and distribution, thereby promoting the creation of densely spherical particles.[25] The TEM images revealed that the nanoparticles displayed nearly spherical morphology with well-defined outlines (Figure 2C). Nanoscale particles with a spherical structure exhibited relatively higher cellular uptake,[26] a requirement met by the prepared nanoparticles in this study. Based on these findings, CCP demonstrated the capability to exist uniformly and stably in aqueous solutions.

DSC

The thermal properties of cas, chrysin, their individual physical blends, and CCPs were assessed through DSC analysis (Figure 2D). Cas presented a broad endothermic peak at 85.81 °C, likely indicative of its fusion. Conversely, a distinct peak at 281.73 °C signified the crystalline state of chrysin. The characteristic peaks observed in the physical mixture demonstrated a straightforward overlay of cas and chrysin. At 88.92 °C, CCPs displayed a broad peak, suggesting a temperature elevation possibly due to the interplay between chrysin and cas.[19] Notably, the CCP spectrum exhibited an endothermic peak resembling cas rather than chrysin, implying that chrysin might have been loaded onto cas in an amorphous form rather than a crystalline form, that similar to former report.[27–29] This observation indicates a departure from chrysin's expected thermodynamic behavior within the chrysin-cas complex.

XRD

The diffraction pattern of cas displayed broad and smooth peaks, indicative of its amorphous structure. Chrysin exhibited distinct and sharp characteristic diffraction peaks at 2θ=25.22°, 28.45°, 30.76°, 35.96°, and 47.30°, indicating its presence in

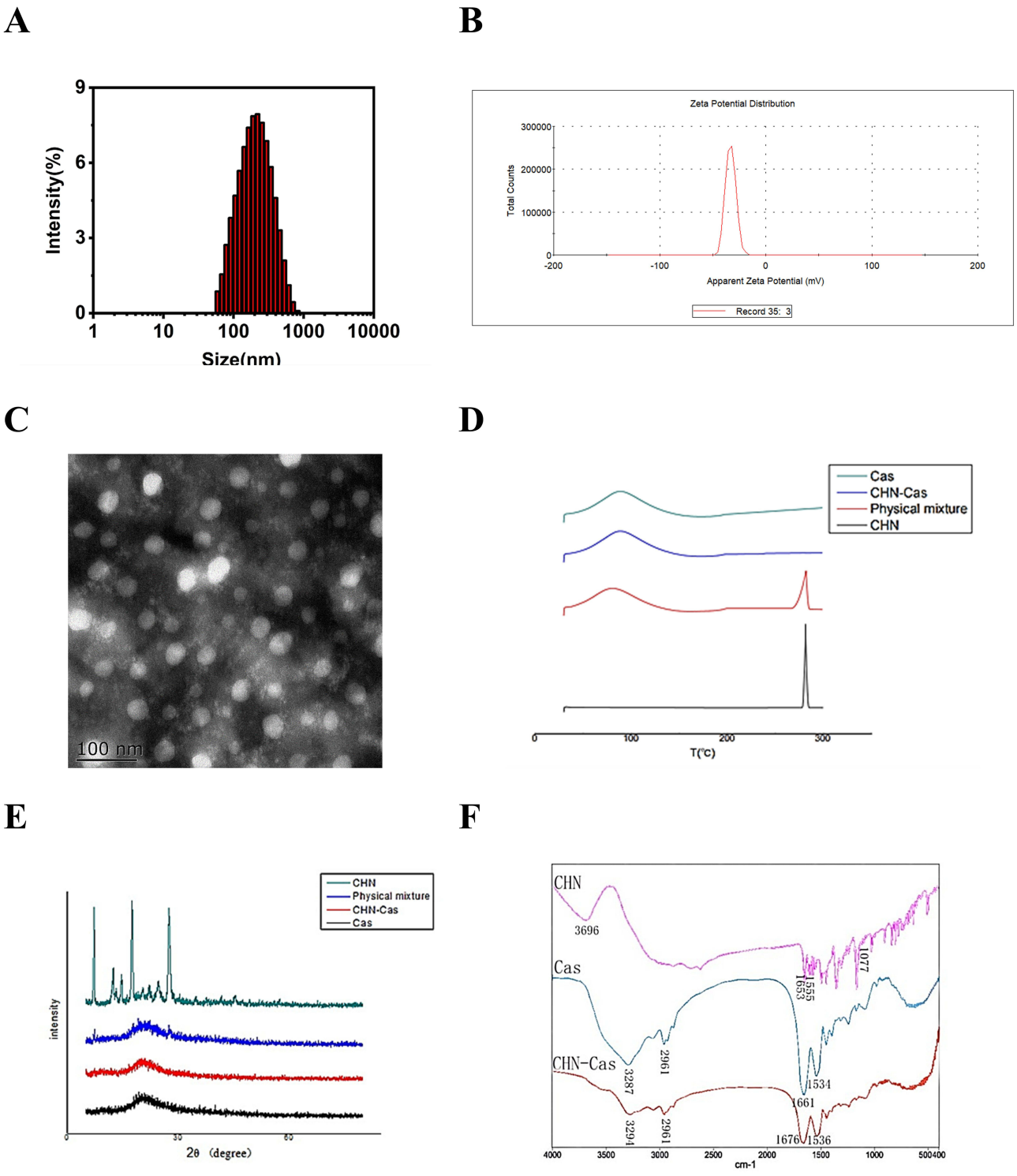

Figure 2 Physicochemical characterization of chrysin-cas nanoparticles. (**A**) Mean particle size (nm) of the prepared nanoparticles. (**B**) Average zeta potential (mV) of the CCPs. (**C**) TEM images of CCPs. (**D**) Differential scanning calorimetry (DSC) thermograms of cas, chrysin, their respective mixtures, and CCPs. (**E**) X-ray diffraction (XRD) patterns of das, chrysin, their respective mixtures, and CCPs. (**F**) Fourier-transform infrared spectroscopy (FTIR) spectra of cas, chrysin, and CCPs.

crystalline form. The diffraction peaks observed in the physical mixture were mainly representative of cas, resulting from a simple summation of chrysin and cas diffraction patterns. Notably, the typical diffraction peaks of chrysin were absent within the CCPs, suggesting chrysin's integration into cas nanoparticles in an amorphous distribution (Figure 2E).

FTIR

The principle of Fourier-transform infrared spectroscopy lies in the detection of infrared light absorption triggered by vibrational transitions within covalent bonds.[26] Analyzing the FTIR spectra of both complexes and their constituent elements enabled the identification of drug-polymer synthesis or reactions. The characteristic bands in the cas spectrum observed at 3287 cm^-1 (OH stretching vibration), 2961 cm^-1 (CH3 stretching vibration), and 1650 cm^-1 (carbonyl C=O stretching vibration) were distinctive. Chrysin's spectrum exhibited specific bands at 3696 cm^-1 (OH stretching vibration), 1653 cm^-1, 1555 cm^-1 (aromatic ring stretching vibration), and 1077 cm^-1 (C-O, C-C-O, C-C stretching vibrations). Notably, the CCP spectrum lacked the absorption peak related to aromatic ring stretching vibration, indicating successful cas embedding within chrysin. Subsequent to chrysin encapsulation by cas for nanoparticle formation, the OH stretching vibration absorption peak shifted from 3287 cm^-1 to 3294 cm^-1, and the C=O stretching vibration absorption peak shifted from 1661 cm^-1 to 1676 cm^-1. These shifts implied the involvement of potential intermolecular forces, such as van der Waals or hydrogen bonding, between the carrier and drug molecules (Figure 2F). These results offered insight into the molecular interactions driving the formation of CCPs. Overlap of the FTIR scans suggested the dominance of cas in the physical blend, compared to chrysin, with more pronounced peaks attributed to cas.[10] In the chrysin-cas nanoparticles, the distinct chrysin peaks exhibited varying degrees of weakening, shifting, or even disappearance, indicating the successful incorporation of chrysin into cas. These results further substantiated that the interaction between cas and chrysin was primarily physical rather than chemical.

In vitro Release Study

The comparative analysis was conducted between chrysin and CCPs within an SDS solution to unveil distinct cumulative release profiles (Figure 3A) former reported methods.[30] The release rate of chrysin from CCP solution was faster than that from chrysin solution. Within the initial 4-hour period, the CCP solution released 81.79% of the compounds, whereas the chrysin solution released only 61.57%. The cumulative release rate of CCP in SDS reached 88.19% ± 5.56%. This phenomenon was ascribed to chrysin's adsorption onto the nanoparticle surfaces, promoting the swift release of a concentrated drug dose upon reaching the target site. With ongoing release, the drug enclosed within the nanoparticles gradually dispersed because the carrier material dissolved, resulting in a relatively slower drug release rate, which enhanced drug efficacy. Consequently, the in vitro release of CCPs complied with biphasic kinetic models (Supplementary Material, Figure S1, Table S2), initially demonstrating rapid drug liberation followed by sustained release.[31]

Pharmacokinetic Studies

The plasma concentration-time curve in Figure 3B illustrates the behavior of chrysin. In vivo, the blood concentration of CCPs escalated rapidly, achieving a maximum blood drug concentration (C_{max}) 1.67 times greater than that of the chrysin

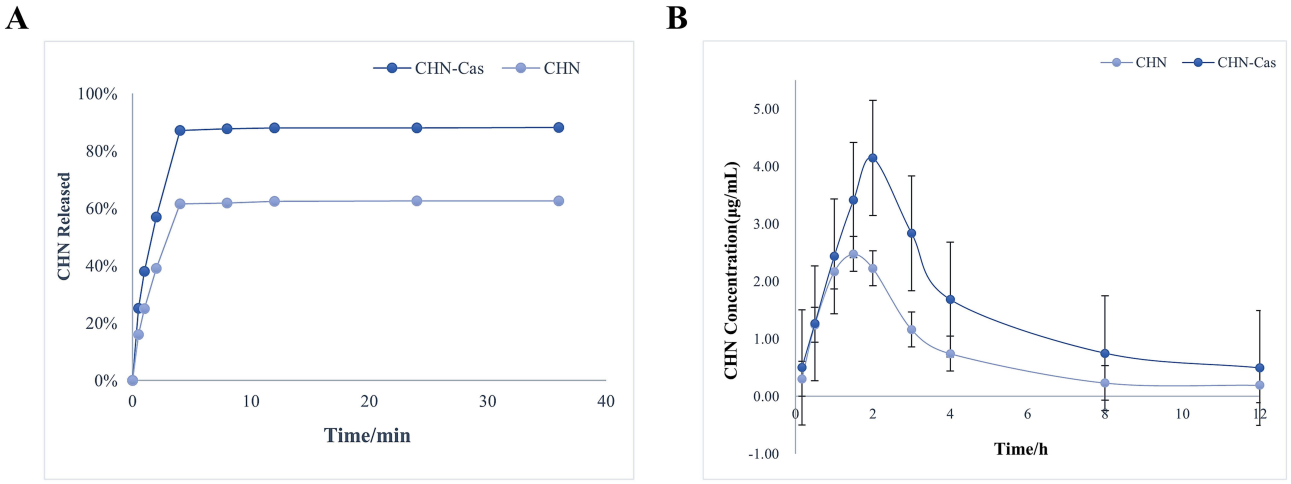

Figure 3 In vitro release and pharmacokinetic study. (**A**) Cumulative release profiles of chrysin and CCPs in vitro. (**B**) Plasma concentration-time curves of chrysin and CCPs.

Table 2 Pharmacokinetic Parameters of Chrysin Following Oral Administration to Mice

Parameters	Units	Mean (Chrysin)	Mean (CCPs)
AUC_{0-12h}	μg/L*h	8.93	17.72
$AUC_{0-\infty}$	μg/L*h	9.14	18.60
T_{max}	h	1.50	2.00
C_{max}	μg/L	2.48	4.15

Notes: $AUC_{0-\infty}$ refers to the area under the concentration-time curve from zero to infinity; $MRT_{0-\infty}$ denotes the mean residence time from zero to infinity.

suspension. Additionally, the overall blood drug concentration of CCPs notably exceeded that of the chrysin suspension. CCPs exhibited a T_{max} of 2.0 hours, whereas the maximum T_{max} of chrysin was 1.5 hours, indicating a distinct sustained-release effect imparted by the nanoparticles. There was a discrepancy in the time taken by CCPs and the chrysin suspension to reach their respective peak plasma concentrations. Notably, the AUC0-∞ of CCPs was 2.01 times higher than that of the chrysin suspension group, as shown in Table 2. The bioavailability of a drug in the body is primarily determined by its solubility, permeability, and dosage.[32] The unique hydrophilic structure of cas, with hydrophilic outer edges and hydrophobic internal cavities, enhanced the solubility of chrysin. Additionally, the CCP complex, characterized by a larger specific surface area, effectively increased the dissolution and release of chrysin by augmenting its contact surface with biological membranes, thereby enhancing its bioavailability.

The Protective Effect of CCP on Lung Infections

After a three-day administration of CCPs, the mice received a single intratracheal dose of Ab and were euthanized 24 hours later. The protective efficacy of CCPs against Ab-induced lung infection was assessed by visually examining pulmonary lesions and assessing lung biomarkers and histopathological alterations. Infection with Ab resulted in lung enlargement and severe congestion (Figure 4A), decreases in mouse body weight (Figure 4B), a marked increase in lung index values (Figure 4C), and elevated total white blood cell counts and neutrophil counts (Figure 4F and G). These findings affirmed the successful establishment of a pulmonary infection model induced by Ab.

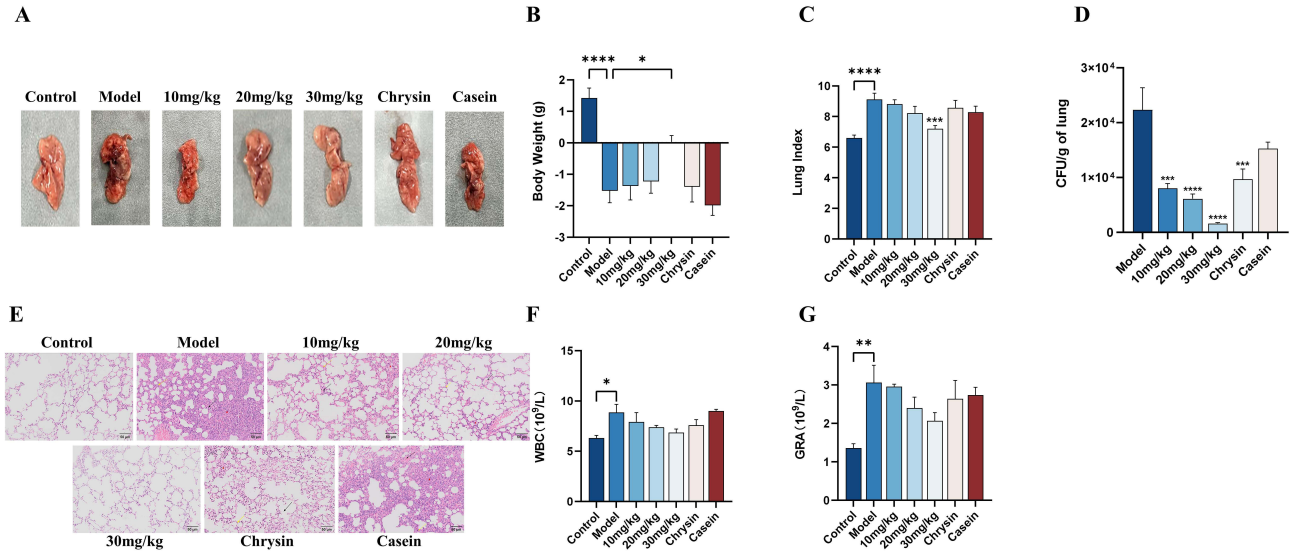

Figure 4 CCP mitigates AB-induced pulmonary infection (**A**), maintains mouse body weight (**B**), and reduces lung index values (**C**) (n = 10) and (**D**) lung bacterial load (n = 5). (**E**) H&E staining of mouse lung tissues (n = 5) (scale bar=50μm). The yellow arrows indicate the thickening of the alveolar septa, the red triangles depict the infiltration of inflammatory cells, and the black arrows signify increased red blood cells. Decreases in WBCs (**F**) and GRA (**G**) levels in the blood (n = 5). Data are presented as the mean ± SEM. Statistical significance was determined using one-way ANOVA. *p < 0.05; **p < 0.01; ***p < 0.001; ****p < 0.0001.

https://doi.org/10.2147/IJN.S457643 DovePress

The administration of high-dose CCPs effectively prevented weight loss in the mice, significantly improved lung conditions, normalized lung index values, and reduced both WBC and monocyte counts in the bloodstream. In the low-dose group, although the data did not show statistical significance, there were slight improvements in lung size, color, and hematological parameters compared to the model group. The chrysin group exhibited drug effects similar to those in the high-dose nanoparticle group, displaying a minor enhancement in lung appearance and a notable decrease in WBC counts. This suggests that chrysin had less therapeutic impact on Ab-induced lung infections when compared with its nano-particle formulation. The encapsulation of CCPs enhanced drug bioavailability and therapeutic effectiveness.

After Ab infection, the mice exhibited significant infiltrations of inflammatory cells, severe hemorrhaging, and noticeably widened alveolar septa in their lungs (Figure 4E). No discernible lung lesions were observed upon treatment with a high dose of CCP. Improvements were evident in the alveolar septa and the extent of inflammatory cell infiltration in the chrysin group compared to the model group.

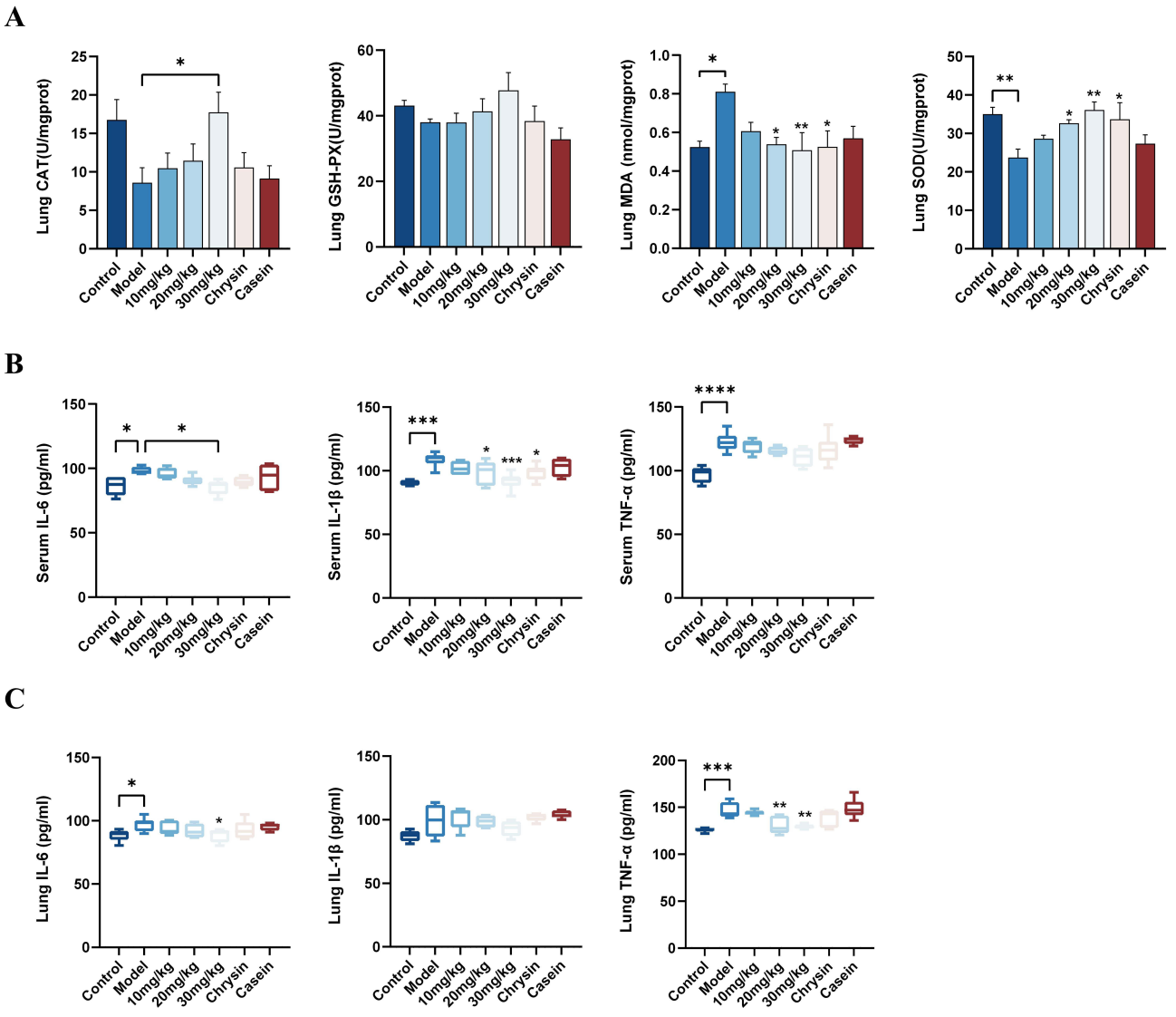

Figure 5 The amelioration of pulmonary oxidative stress and inflammatory factors by CCP. Levels of SOD, CAT, GSH-PX, and MDA in mouse lung tissues (**A**). CCP reduced the levels of IL-6, IL-1β, and TNF-α in the serum (**B**) and lung tissues (**C**) of mice in the model group. The results are presented as the mean ± standard error of the mean (SEM), analyzed using one-way ANOVA. *p < 0.05, **p < 0.01, ***p < 0.001, and ****p < 0.0001 indicate statistically significant differences.

As shown in Figure 4D, compared to the model group, both the CCP and chrysin groups exhibited a significant reduction in lung bacterial load. The high-dose CCP group also showed a notably lower lung bacterial load compared to the chrysin group, indicating that CCPs were more effective in preventing bacterial colonization than chrysin alone.

The levels of MDA, GSH-PX, CAT, and SOD were assessed to explore the impact of CCPs on oxidative stress induced by Ab lung infection (Figure 5A). The results revealed decreased levels of lung antioxidant enzymes in the model group when compared with control group, indicating the presence of oxidative stress. SOD and CAT levels were increased, and MDA levels were decreased in the high-dose CCP group comparing to model group. SOD levels in the high-dose CCP group were significantly higher than those in the chrysin group. Although not statistically significant, GSH-PX levels displayed a rising trend, particularly with high-dose CCP administration.

Cellular cytokines play a pivotal role in inflammation and host defenses against bacterial infections. Studies have highlighted substantial elevations in cytokine levels during Ab infection, indicating their critical involvement in the infectious process.[33] Ab infection triggers the production of IL-6, IL-1β, and TNF-α within the lungs, contributing significantly to severe pulmonary pathogenesis.[34] ELISA kits were utilized to measure the levels of IL-6, IL-1β, and TNF-α in serum and lung tissue samples (Figure 5B and C). The secretion of pro-inflammatory cytokines was increased in the model group compared to the control group. However, CCPs demonstrated effective anti-inflammatory activity by suppressing the production of these pro-inflammatory cytokines.

Conclusion

CCPs addressed the low oral bioavailability issue of other chrysin formulations. This study effectively synthesized CCPs by a straightforward, practical preparation process and yielded safe and effective outcomes without complexity. CCPs exhibited sustained-release characteristics in an SDS solution, prolonging the drug's efficacy. In vivo experiments showed that CCPs suppressed oxidative stress and pro-inflammatory cytokine activity significantly more than free chrysin. These comprehensive experimental findings underscore CCPs as a novel drug delivery system with improved water solubility and enhanced bioavailability, promising extensive applications in the medical field.

Data Sharing Statement

The data that support the findings of this study are available from the corresponding author upon reasonable request.

Acknowledgments

Huaqiao Tang, Liying Dong and Xue Xia are co-first authors for this study. The authors thank Sichuan Agricultural University for providing the necessary experimental equipment.

Disclosure

The authors disclose no potential conflicts of interest.

References

1. Jafari S, Dabiri S, Mehdizadeh Aghdam E. Synergistic effect of chrysin and radiotherapy against triple-negative breast cancer (TNBC) cell lines. *Clin Transl Oncol*. 2023;25(8):2559–2568. doi:10.1007/s12094-023-03141-5
2. Shen Y, Tian P, Li D. Chrysin suppresses cigarette smoke-induced airway inflammation in mice. *Int J Clin Exp Med*. 2015;8(2):2001–2008.
3. Chen M, Li J, Liu X. Chrysin prevents lipopolysaccharide-induced acute lung injury in mice by suppressing the IRE1α/TXNIP/NLRP3 pathway. *Pulm Pharmacol Ther*. 2021;68:102018. doi:10.1016/j.pupt.2021.102018
4. Ting P, Srinuanchai W, Suttisansanee U, et al. Development of chrysin loaded oil-in-water nanoemulsion for improving bioaccessibility. *Foods*. 2021;10:8.
5. Jin P, Yao R, Qin D, Chen Q, Du Q. Enhancement in antibacterial activities of eugenol-entrapped ethosome nanoparticles via strengthening its permeability and sustained release. *J Agricult Food Chem*. 2019;67(5):1371–1380. doi:10.1021/acs.jafc.8b06278
6. Elzoghby AO, El-Fotoh WS, Elgindy NA. Casein-based formulations as promising controlled release drug delivery systems. *J Control Release*. 2011;153(3):206–216.
7. Shapira A, Markman G, Assaraf YG, Livney YD. Beta-casein-based nanovehicles for oral delivery of chemotherapeutic drugs: drug-protein interactions and mitoxantrone loading capacity. *Nanomedicine*. 2010;6(4):547–555. doi:10.1016/j.nano.2010.01.003
8. Pereira PC. Milk nutritional composition and its role in human health. *Nutrition*. 2014;30(6):619–627. doi:10.1016/j.nut.2013.10.011
9. Turovsky T, Portnaya I, Kesselman E, et al. Effect of temperature and loading on the structure of β-casein/ibuprofen assemblies. *J Colloid Interface Sci*. 2015;449:514–521. doi:10.1016/j.jcis.2015.02.030

10. Elzoghby AO, Helmy MW, Samy WM, Elgindy NA. Spray-dried casein-based micelles as a vehicle for solubilization and controlled delivery of flutamide: formulation, characterization, and in vivo pharmacokinetics. *Eur. J. Pharm. Biopharm.* 2013;84(3):487–496. doi:10.1016/j.ejpb.2013.01.005
11. Elzoghby AO, Elgohary MM, Kamel NM. Implications of protein- and Peptide-based nanoparticles as potential vehicles for anticancer drugs. *Adv Protein Chem Struct Biol*. 2015;98:169–221.
12. Knirel YA, Shneider MM, Popova AV. Mechanisms of Acinetobacter baumannii capsular polysaccharide cleavage by phage depolymerases. *Biochem Biokhimiia*. 2020;85(5):567–574. doi:10.1134/S0006297920050053
13. Higham SL, Baker S, Flight KE. Intranasal immunization with outer membrane vesicles (OMV) protects against airway colonization and systemic infection with Acinetobacter baumannii. *J Infect*. 2023;86(6):563–573. doi:10.1016/j.jinf.2023.02.035
14. Cai Y, Chai D, Wang R, Liang B, Bai N. Colistin resistance of Acinetobacter baumannii: clinical reports, mechanisms and antimicrobial strategies. *J Antimicrob Chemother*. 2012;67(7):1607–1615. doi:10.1093/jac/dks084
15. Zhao Y, Liu Y, Feng L. In vitro and in vivo synergistic effect of chrysin in combination with colistin against Acinetobacter baumannii. *Front Microbiol*. 2022;13:961498. doi:10.3389/fmicb.2022.961498
16. Shapira A, Davidson I, Avni N, Assaraf YG, Livney YD. β-Casein nanoparticle-based oral drug delivery system for potential treatment of gastric carcinoma: stability, target-activated release and cytotoxicity. *Eur. J. Pharm. Biopharm.* 2012;80(2):298–305. doi:10.1016/j.ejpb.2011.10.022
17. Palamoor M, Jablonski MM. Synthesis, characterization and in vitro studies of celecoxib-loaded poly(ortho ester) nanoparticles targeted for intraocular drug delivery. *Colloids Surf. B*. 2013;112:474–482. doi:10.1016/j.colsurfb.2013.07.039
18. Bachar M, Mandelbaum A, Portnaya I. Development and characterization of a novel drug nanocarrier for oral delivery, based on self-assembled β-casein micelles. *J Control Release*. 2012;160(2):164–171. doi:10.1016/j.jconrel.2012.01.004
19. Modarres-Gheisari SMM, Gavagsaz-Ghoachani R, Malaki M, Safarpour P, Zandi M. Ultrasonic nano-emulsification - A review. *Ultrason Sonochem*. 2019;52:88–105. doi:10.1016/j.ultsonch.2018.11.005
20. Gandhi S, Roy I. Doxorubicin-loaded casein nanoparticles for drug delivery: preparation, characterization and in vitro evaluation. *Int J Biol Macromol*. 2019;121:6–12. doi:10.1016/j.ijbiomac.2018.10.005
21. Santo Pereira AE, Silva PM, Oliveira JL, Oliveira HC, Fraceto LF. Chitosan nanoparticles as carrier systems for the plant growth hormone gibberellic acid. *Colloids Surf B*. 2017;150:141–152. doi:10.1016/j.colsurfb.2016.11.027
22. Sydow S, de Cassan D, Hänsch R. Layer-by-layer deposition of chitosan nanoparticles as drug-release coatings for PCL nanofibers. *Biomater. Sci.* 2018;7(1):233–246. doi:10.1039/c8bm00657a
23. Shapira A, Assaraf YG, Epstein D, Livney YD. Beta-casein nanoparticles as an oral delivery system for chemotherapeutic drugs: impact of drug structure and properties on co-assembly. *Pharm Res*. 2010;27(10):2175–2186. doi:10.1007/s11095-010-0222-7
24. Guerra-Rosas MI, Morales-Castro J, Ochoa-Martínez LA, Salvia-Trujillo L, Martín-Belloso O. Long-term stability of food-grade nanoemulsions from high methoxyl pectin containing essential oils. *Food Hydrocoll*. 2016;52(0268):438–446.
25. Yang M, Wei Y, Ashokkumar M, Qin J, Han N, Wang Y. Effect of ultrasound on binding interaction between emodin and micellar casein and its microencapsulation at various temperatures. *Ultrason Sonochem*. 2020;62:104861. doi:10.1016/j.ultsonch.2019.104861
26. Dhandapani RK, Gurusamy D, Howell JL, Palli SR. Development of CS-TPP-dsRNA nanoparticles to enhance RNAi efficiency in the yellow fever mosquito, Aedes aegypti. *Sci Rep*. 2019;9(1):8775. doi:10.1038/s41598-019-45019-z
27. Loo C-Y, Traini D, Young PM, Parumasivam T, Lee W-H. Pulmonary delivery of curcumin and quercetin nanoparticles for lung cancer–Part 1: aerosol performance characterization. *J Drug Delivery Sci Technol*. 2023;86:104646. doi:10.1016/j.jddst.2023.104646
28. Wang L, Jia W, Yang Q, Cai H, Zhao X. Casein nanoparticles as oral delivery carriers for improved bioavailability and hypoglycemic activity of apigenin. *Food Hydrocoll*. 2024;1:146.
29. Liang Q, Sun X, Raza H, Khan MA, Ma H, Ren X. *Fabrication and Characterization of Quercetin Loaded Casein PhosphopeptidesChitosan Composite Nanoparticles by Ultrasound Treatment: Factor Optimization, Formation Mechanism, Physicochemical Stability and Antioxidant Activity*. Social Science Electronic Publishing; 2021.
30. Lee W-H, Bebawy M, Loo C-Y, Luk F, Mason RS, Rohanizadeh R. Fabrication of curcumin micellar nanoparticles with enhanced anti-cancer activity. *J Biomed Nanotechnol*. 2015;11(6):1093–1105. doi:10.1166/jbn.2015.2041
31. Matshetshe KI, Parani S, Manki SM, Oluwafemi OS. Preparation, characterization and in vitro release study of β-cyclodextrin/chitosan nanoparticles loaded Cinnamomum zeylanicum essential oil. *Int J Biol Macromol*. 2018;118(Pt A).
32. Fine-Shamir N, Beig A, Miller JM, Dahan A. The solubility, permeability and the dose as key factors in formulation development for oral lipophilic drugs: maximizing the bioavailability of carbamazepine with a cosolvent-based formulation. *Int J Pharm*. 2020;582:119307. doi:10.1016/j.ijpharm.2020.119307
33. Zhou Y, Xiang C, Wang N. Acinetobacter baumannii reinforces the pathogenesis by promoting IL-17 production in a mouse pneumonia model. *Med Microbiol Immunol*. 2023;212(1):65–73. doi:10.1007/s00430-022-00757-2
34. Harris G, KuoLee R, Xu HH, Chen W. Acute intraperitoneal infection with a hypervirulent Acinetobacter baumannii isolate in mice. *Sci Rep*. 2019;9(1):6538. doi:10.1038/s41598-019-43000-4